



## Experimental and modeling analysis of lignin derived polymer in flocculating aluminium oxide particles



Minoos Ataie<sup>a</sup>, Kayte Sutherland<sup>a</sup>, Leila Pakzad<sup>a</sup>, Pedram Fatehi<sup>a,b,\*</sup>

<sup>a</sup> Green Processes Research Centre and Department of Chemical Engineering, Lakehead University, Thunder Bay, ON P7B 5E1, Canada

<sup>b</sup> State Key Laboratory of Biobased Material and Green Papermaking/Key Lab of Pulp & Paper Science and Technology of Education Ministry of China, Qilu University of Technology (Shandong Academy of Sciences), Jinan, Shandong Province 250353, China

### ARTICLE INFO

#### Keywords:

Aluminium oxide  
Suspension  
Flocculation  
Kraft lignin  
Numerical modeling

### ABSTRACT

This study involves the experimental evaluation of flocculation systems for aluminium oxide particles using a semi-natural flocculant, kraft lignin-acrylic acid (KL-AA) polymer, with sophisticated tools, such as focused beam reflectance measurement and vertical scanner analyzer. A novel statistical framework was also developed to model the experimental results, which led to a more in-depth analysis of shape and size of flocs in heterogeneous suspensions. The mathematical modeling of the generated results revealed that the polymer induced generally larger flocs with three different size regimes. The weak interaction of KL-AA and the particles generated the largest but loosely structured flocs (with the greatest deviation from a spherical shape) at pH 3. These flocs could not be recovered after de-flocculation/re-flocculation, they had the slowest settling performance and they made sediment with the lowest concentration at pH 3. The charge interaction and bridging mechanisms generated flocs with the largest recoverable size after de-flocculation/re-flocculation at pH 6. The generated flocs became more compact and spherical as pH increased in the system. Interestingly, with increasing salinity of the system, the polymer induced larger flocs with a less compact structure. The flocs seemed to be slightly stronger at higher salinity, they settled in faster pace, and they made more compact sediments.

### 1. Introduction

Flocculation plays an important role in solid-liquid separation processes used in different industries for applications such as sedimentation, thickening, flotation, and filtration. Flocculants are also used heavily in mineral processing, water treatment and sludge dewatering [58,60]. In recent years, different flocculants, especially synthetic polymers, have been developed and applied to promote the settling of the colloidal particles in suspension systems [3]. It was reported that polyacrylamide (PAM) and its derivatives are widely used as flocculants [4,45]. However, the high cost and non-biodegradability of PAM have led to growing interests in developing environmentally friendly flocculants [35].

Lignin is an abundant natural product that is commercially produced as a waste in conventional pulping processes, such as the well-known kraft process. Lignin has a three-dimensional aromatic complex structure with several functional groups, such as carboxyl, hydroxyl, methoxy, and aldehyde [7]. To generate large anionic lignin-based polymers, some studies have focused on the polymerization of lignin with acrylate monomers [38,14,53,49,37,61]. In our previous work, for

example, kraft lignin (KL) was modified with acrylic acid (AA) in an acidic aqueous suspension system to produce a kraft lignin-acrylic acid (KL-AA) polymer with a high molecular weight and anionicity, and the polymer appeared to be a promising candidate for flocculating particles in suspension systems [24,32,33]. The previous studies showed promising flocculation performance of KL-AA for different systems [23,54;17]. The present work is the continuation of those studies to understand the fundamentals of the flocculation performance and floc properties of KL-AA as promising flocculant for an aluminium oxide-based suspension.

In flocculation systems, the performance of flocs is significantly affected by the molecular weight, charge density and dosage of the polymers as well as the size of suspended particles, the ionic strength and pH of the suspension [59]. Since the floc characteristics have a pronounced influence on the dewatering processes, studies have focused on establishing a relationship between the characteristics and performance of flocculants with respect to the settling and dewatering behavior of the induced flocs in colloidal systems [41,40,20,44]. In the past, it was reported that adjusting the pH of the suspension had a significant effect on the floc size, strength, and structure, which

\* Corresponding author at: Green Processes Research Centre and Department of Chemical Engineering, Lakehead University, Thunder Bay, ON P7B 5E1, Canada.  
E-mail address: [pfatehi@lakeheadu.ca](mailto:pfatehi@lakeheadu.ca) (P. Fatehi).

impacted the efficiency of solid/liquid separation systems greatly [48]. For example, Rattanakawin and Hogg [48] reported that the flocs produced via the coagulation of aluminium oxide particles were the largest for a solution at pH 8.6. Other solution acidities led to smaller flocs due to the electrostatic repulsion force developed between the particles [48]. Cao et al. [8] reported that flocs formed with the addition of poly-ferric chloride (PFC) in the treatment of water were larger at a neutral pH than other pH.

Additionally, the strength of flocs was reported to decrease with reducing pH. In one study, intensifying the shear rates increased floc's compactness and decreased its recovery capability for a solution at pH 4. At natural and alkaline conditions, flocs were observed to have an improved re-growth capability [8]. Tambo and Hozumi [50] reported that the settling rate of particles was augmented with floc strength. According to Francois [19], an increase in the number of particles forming the flocs would decrease the bonding strength and stability of the aggregates. It has also been reported that floc strength was inversely related to flocs size [50], reflecting that larger flocs would be subjected to more breakdown under shear forces since the probability of possessing weaker bonds in the floc structure would increase [57]. Furthermore, larger-sized flocs have a more porous structure which increases the vulnerability of the flocs to breakage [57].

The primary objective of the current work was to study the effects of suspension pH and salinity on the performance of KL-AA polymer when it was used as a flocculant for aluminium oxide suspension. Prior studies have indicated that mathematical modeling could be used as a powerful tool to correlate factors affecting flocculation [52]. The mathematical models used in this work are used to quantify the influences of parameters, such as solution pH, salinity and mixing intensity, on the flocculation. These factors affect the dynamics of floc formation, flocs size, dewatering, and compressibility [52]. In particular, this work studies the kinetics of flocculation through first-order modeling of the system response to determine gain and time constant. A probabilistic mathematical model was also used to estimate the heterogeneity of floc shape as a form of shape analysis for the flocs. A non-invasive analysis technique, focused beam reflectance measurement (FBRM), was used to study the impact of agitation speed on the median floc size. A vertical scan analyzer was also utilized to study the flocculation and settling process of the KL-AA aluminium oxide systems in non-stirring conditions. The main novelty of this work was the mathematical modeling of floc structures and flocculation systems on the experimental results obtained for a newly developed lignin-based flocculant in aluminium oxide systems.

## 2. Materials and methods

### 2.1. Materials

Al<sub>2</sub>O<sub>3</sub> particles were purchased from Beta Diamond Products Inc., Yorba Linda, CA, and were used for the preparation of the test suspension. The KL-AA polymers were prepared from acrylic acid (AA) and softwood kraft lignin (KL). A KL sample was provided by FPInnovations from its pilot plant in Thunder Bay, ON, Canada. In our experiments, the analytical grades of the following chemicals were purchased from Sigma-Aldrich and used without further purification: acrylic acid (AA), NaCl, poly diallyl dimethyl ammonium chloride (PDADMAC, 100–200 kg/mol), sodium azide NaN<sub>3</sub> (99.5%), NaNO<sub>3</sub>, D<sub>2</sub>O, trimethylsilyl propanoic acid (TSP) as internal standard, HCl (0.1 M), NaOH (97%), and H<sub>2</sub>SO<sub>4</sub> (98%). Dialysis membrane (cut off of 1000 g/mol) was obtained from Spectrum company.

### 2.2. Polymerization and characterization of KL-AA

The polymerization of KL and AA was conducted, as explained in the [supplementary material](#). Also, the charge density, molecular weight, carboxylate group and structure of KL-AA were

comprehensively analyzed using advanced tools. The details of these investigations are provided in the [supplementary material](#).

### 2.3. Zeta potential analysis

The zeta potential of aluminium oxide suspensions containing KL-AA was measured by an electrophoresis technique using a zeta potential analyzer (NanoBrook Omni, Brookhaven Instruments) following a previous work's methodology [31]. Different dosages of KL-AA and aluminium oxide suspensions were mixed to generate aluminium oxide/KL-AA systems at various ratios. After placing in a water bath (150 rpm, 30 °C, 1 h duration), the suspension samples were diluted with a 1 mM KCl solution before the zeta potential analysis. This experiment was repeated at pH 3, 6 and 9.

### 2.4. Flocculation analysis

#### 2.4.1. Analysis under mixing conditions

The flocculation process of aluminium oxide particles and KL-AA, as well as the produced floc properties, were analyzed by a focused beam reflectance measurement (FBRM, Mettler-Toledo E25). The FBRM with a diameter of 25 mm was used for the analysis via scanning a highly focused beam at a fixed speed (2 m/s) across a particle in suspensions. In this analysis, the chord length of particles, which is the distance between the two edges of particles, was measured by a multiplying duration of reflectance from particles by the optical rotating speed of the laser scanner [18]. In this work, the focal point was set to be  $-20 \mu\text{m}$  [6] and scan intervals were set at 10 s. In this set of experiments, the FBRM probe was immersed in 200 g of suspension (25 g/L, pH 6 and NaCl concentrations of 0 mM, 10 mM, and 100 mM). The FBRM equipment was calibrated with standard polyvinyl alcohol particles provided by the FBRM manufacturer.

Trials were carried out to study the effect of KL-AA type and dosage on the size and floc properties. In this set of experiments, consecutive dosages of KL-AA were added when the signal of the FBRM was stable. While stirring aluminium oxide suspension (25 g/L, pH 6) at 300 rpm, the first dosage of KL-AA (0.2 mg/g) was added and the addition was continued to 20 mg/g of KL-AA in the system. To investigate the effect of shear forces on flocculation, the analysis was conducted with 200 g of aluminium oxide suspension (25 g/L), at pH of 3, 6 and 9, and NaCl concentrations of 0, 10, 100 mM. First, the aluminium oxide suspension was stirred at 300 rpm for 200 s. Then, KL-AA in its optimal dosage was introduced and allowed the flocs to form for a period of 400 s at 300 rpm. Then, stirring intensity was increased to 600 rpm for 200 s to study the de-flocculation. Finally, the stirring intensity was reduced to 300 rpm to re-flocculate the broken flocs in the suspension.

#### 2.4.2. De-flocculation and re-flocculation indices

De-flocculation and re-flocculation indices are used to study the stability of flocs under increased shear forces and the affinity of flocs to re-grow after decreasing shear forces. Eqs. (1) and (2) provide the means for determining the de-flocculation and re-flocculation indices, respectively:

$$DI(\%) = \frac{x_4 - x_3}{x_3 - x_1} \times 100\% \quad (1)$$

$$RI(\%) = \frac{x_5 - x_4}{x_3 - x_1} \times 100\% \quad (2)$$

where  $x_1$  is the stable median chord length before polymer addition,  $x_3$  is the stable median chord length after polymer addition and before increasing shear forces,  $x_4$  is the minimum of the stable median chord length subjected to shear forces, and  $x_5$  is the maximum of the stable median chord length after decreasing shear forces [42]. FBRM analysis was used to examine the median chord lengths of the systems for use in Eqs. (1) and (2).

2.4.3. Estimation of floc shape via probabilistic modeling

The shape of flocs formed during aggregation processes may be described via knowledge of a characteristic length (such as chord length) and knowledge of a fractal dimension, which relates the characteristic length of a particle to an aspect of its geometry (i.e., perimeter, surface area, or volume) [11]. The fractal dimension is necessary to correlate characteristic length with shape; knowing merely the characteristic length does not necessarily provide information concerning the two- or three-dimensional shape the characteristic length is derived from. For example, one cannot determine if a shape is spherical or cylindrical if merely provided a diameter. The process of determining the shape of flocculant particles and aggregate flocs is complicated since stirring conditions result in simultaneous breakage and re-flocculation processes, thus more than one size and shape of flocs may be observed in the system and these shapes change overtime. A mathematical approach may facilitate the study of complex heterogeneous systems by classifying suspended particles into a finite number of identical particle regimes (i.e., clusters), in which the particles indicate relatively more tractable behavior for the purpose of shape analysis. This simplification is more manageable than a potentially infinite variety of shapes and will provide an indication of the number of clusters a suspended particle's shape falls under, providing information concerning the uniformity of shapes.

The following model estimates cumulative chord length distribution as a function of the shape clusters for a flocculation system. The number of shape clusters are altered such that the probabilistic model fits the experimental chord length distributions. The process of fitting a theoretical probability distribution to an empirical distribution involves reducing the difference between each such that the theoretical distribution mimics the empirical data. A measure of how different a given probability distribution is from a reference distribution is indicated through the Kullback-Leibler divergence [34]. In this study, by minimizing  $D_{KL}(\mathbf{p} \parallel \hat{\mathbf{p}})$  (the Kullback-Leibler divergence), one can find a vector  $\mathbf{p} = [p_1, \dots, p_m]^T$  of probabilities such that the theoretical probability distribution fits the empirical chord length distribution provided by the FBRM analysis.

First, a time-indexed sequence is assumed  $\{x_t\}_{t_0}^{t_0+\tau}$  a time frame, whose chord length quantities the recorded ones by FBRM at  $n$  given time points. In this frame,  $t \in [t_0, t_0 + \tau]$  where  $\tau > 0$  denotes the total duration of the experiment. The main goal of the shape analysis is to employ the provided time frame to identify a set of attributes that can effectively characterize the particle geometrics. In practice, however, one does not usually have access to the complete  $\{x_t\}_{t_0}^{t_0+\tau}$  for  $n$  measurements. This is mainly due to the existence of a large volume of records gathered by FBRM, whose process would require the development of specific methodologies to overcome the memory-related limitations [10]. For this reason, it is often more practical to deal with various summary statistics of the measurements rather than employing their actual values  $\{x_t\}_{t_0}^{t_0+\tau}$ .

Among different summary statistics provided by FBRM, the frequency distribution of measurements has found a wide range of applications. This frequency distribution, which is also referred to as chord length distribution (CLD), could be seen as a histogram, which counts the number of observations that fall into the predefined disjoint chord length bin categories of length. In this case, it is assumed that each chord length result belongs to one and only one of the following  $m$  disjoint chord length channel of:

- $(b_0, b_1]$ ,
- $(b_1, b_2]$ ,
- $\vdots$
- $(b_{j-1}, b_j]$ ,
- $\vdots$

$(b_{m-1}, b_m]$

where  $b_{j-1}$  and  $b_j$  denote left and right boundaries of the  $j$ th channel. The probability that exactly  $z_j$  measurements of FBRM fall into  $(b_{j-1}, b_j]$  for all  $j \in \{1, 2, \dots, m\}$  is given by the following multinomial distribution (Eq. (3)) [48]:

$$\mathbb{P}(Z_1 = z_1, \dots, Z_j = z_j, \dots, Z_m = z_m; \mathbf{p}) = \frac{n!}{z_1! \dots z_j! \dots z_m!} p_1^{z_1} \dots p_j^{z_j} \dots p_m^{z_m} \quad (3)$$

where the vector  $Z = [z_1, \dots, z_m]^T$  is the total count of particles of realizations of the random variable of  $Z_1, \dots, Z_m$  that satisfy the relationship of Eq. (3a):

$$\sum_{j=1}^m z_j = n \quad (3a)$$

and the term  $p_j$  denotes the probability that outcomes of the random experiment would belong to interval  $(b_{j-1}, b_j]$  for every  $j = \{1, 2, \dots, m\}$  such that equation (3b) is true:  $\sum_{j=1}^m p_j = 1$

$$\sum_{j=1}^m p_j = 1 \quad (3b)$$

Via optimization of Eq. (4), the number of clusters underlying the frequency distribution of the measured chord lengths and the parameters governing each cluster can be obtained (Eq. (4)):

$$\min_{\varepsilon, \delta, \pi} D_{KL}(\mathbf{p} \parallel \hat{\mathbf{p}}) = - \sum_{j=1}^m \hat{p}_j \log \left( \frac{p_j(\varepsilon, \delta, \pi)}{\hat{p}_j} \right) \quad (4)$$

$$\text{s. t. } \sum_{i=1}^{\kappa} \pi_i = 1 \quad i = 1, 2, \dots, \kappa;$$

$$\pi_i \in [0, 1] \quad i = 1, 2, \dots, \kappa;$$

$$\varepsilon_i \in (1, \infty) \quad i = 1, 2, \dots, \kappa;$$

$$\delta_i \in (0, \infty) \quad i = 1, 2, \dots, \kappa.$$

where  $\mathbf{p}$  is a vector of probabilities,  $\hat{\mathbf{p}}$  is the observed proportion of measured counts by FBRM,  $m$  is the number of disjoint chord length channel,  $\kappa$  denotes the number of underlying clusters,  $\pi$  is the observed proportion of each cluster,  $\varepsilon$  is elongation and  $\delta$  is semi-axis of a prolate spheroid. The constraint of the model described by Eq. (3) is linear and its objective function is a non-linear, which is differentiable in  $0 < x < \varepsilon_i \delta_i$  except at finite number of points where  $x = \delta_i$  for  $i = 1, 2, \dots, \kappa$ .

To analyze the theoretical number of shape clusters through the fitting of Eq. (4) to experimental FBRM chord length-count distributions, experiments were conducted at pH of 3, 6, and 9 and in NaCl concentrations of 0 and 100 mM at a stirring speed of 300 rpm. A code was generated in Python script for the model. The number of clusters was altered to further minimize the Kullback-Leibler divergence (Eq. (3)) until the lowest divergence was obtained. The cluster condition producing the lowest Kullback-Leibler divergence between the theoretical and experimental distributions was considered to be the most correct and therefore the estimative of the heterogeneity in floc shapes.

2.5. Flocculation under non-stirring conditions

In this analysis, the flocculation and sedimentation behavior of aluminium oxide particles under gravitational non-stirring (i.e., settling with gravity) conditions in the absence or presence of KL-AA was studied by a vertical scan analyzer, Turbiscan (Lab Expert, Formulaction). Silicon standard with the transmission of 99.5% and Teflon standard with the backscattering of 54.5%, which were supplied by the manufacturer, were used for instrument calibration.

In this set of experiments, KL-AA was added to the aluminium oxide suspension (25 g/L) at the optimum dosage. Then, 20 mL of the

suspensions were placed in a cylindrical glass cell of the instrument. The cylindrical glass cell was scanned at each 40  $\mu\text{m}$  intervals with electro luminescent diode light at 880 nm [25]. The scanning was performed every 25 s and the analysis lasted for 1 h.

To determine the overall effect of KL-AA addition on the stability of  $\text{Al}_2\text{O}_3$  suspension, the stability coefficient (TSI, Turbiscan Stability Index) was determined for the suspensions. This indicator considers all processes occurring in the suspension and the value of TSI is calculated from their average values [15]:

$$TSI = \sqrt{\frac{\sum_{i=1}^n (\alpha_i - \alpha)^2}{n - 1}} \quad (5)$$

where  $\alpha_i$  is the average backscattering for each minute of measurement, and  $n$  is the number of scans. In the flocculation analysis, the flocs, which were produced by KL-AA, would settle at different rates. This settlement would clear up the top part of the cell, while generating a layer of sediment at the bottom of the cell. The transmission information gathered from the top layer after settling for 1 h was used for calculating the flocculation efficiency of KL-AA on aluminium oxide suspension. The backscattering and transmission data was gathered as a function of the height of the sample [39,27]. The backscattering data, which was gathered from the bottom part of the cell, was considered for evaluating the sediment thickness. The ratio of the mass to volume for settled flocs after 1 h of settling analysis was used for determining the compactness of the sediment. The concentrations of particles in the sample, which were collected from supernatant parts of the sample before and after adding KL-AA, was calculated while drying at 102 °C overnight. The rate of sediment thickness growth (as a function of time) can be used for determining the settling velocity of flocs.

### 3. Results and discussion

#### 3.1. Zeta potential of suspension

The produced KL-AA had carboxylate group of 4.2 mmol/g, charge density of  $-4.4$  meq/g and molecular weight ( $M_w$ ) of 2800 kg/mol. The zeta potential is used to evaluate the strength of the electrostatic forces of the suspensions [36]. Electrostatic neutralization plays an important role in the interaction of particles and oppositely charged polymers [9,41]. Fig. 1 shows the zeta potential of aluminium oxide suspension as a function of the dosage of KL-AA in various pH of 3, 6 and 9. The zeta potential of the aluminium oxide suspensions without

KL-AA was +49, +30 and  $-5$  mV at pH values of 3, 6, and 9, respectively, which depicts that aluminium oxide suspensions at pH 3 and 6 were stable, but it was unstable at pH 9. The aggregation of aluminium oxide particles in the absence of KL-AA is mostly controlled by electrostatic repulsion between the particles, which is minimum at zero zeta potential of aluminium oxide (pH = 8.6) [16]. Aluminium oxide particles are negatively charged at pH 9, but the degree of the electrostatic repulsive forces is low to cause complete stabilization. The addition of KL-AA decreased the zeta potential of the suspension at all pH values, and this trend is more evident at pH 6. The pKa of polyacrylic acid (PAA) was reported to be 4.5 [21]. Generally, associated carboxyl group participates in hydrogen bonding below pKa value, while the dissociated one is responsible for electrostatic interaction when the pH exceeds the pKa value [21]. Under acidic conditions, associated carboxyl groups interact with aluminium oxide's surface through hydrogen bonding [21]. The slight reduction in the zeta potential at pH 3 is due to the fact that the particles are cationically charged but the carboxylate group of KL-AA are protonated with a limited anionic charge minimally impacting the zeta potential. At pH 6, the particles are still cationically charged, but the KL-AA are anionically charged and their presence and consecutive dosage remarkably impacts the zeta potential. At higher than isoelectric point (pH = 8.6), both aluminium oxide particles and KL-AA are negatively charged and the repulsion force in the system is enhanced gradually via adding KL-AA.

#### 3.2. Flocculation under dynamic conditions

##### 3.2.1. Impact of dosage on flocculation

Fig. 2 shows the median chord length of aluminium oxide particles in the presence of KL-AA for solutions with varied pH. In this figure, the peaks of chord length occurred when consecutive dosages (in the range of 0.2–20 mg/g) of KL-AA were added to the suspensions. Hydro-dynamically induced shear is the main driving force for the flocculation process in orthokinetic agglomeration of particles [43]. As flocculation is a dynamic process, growing flocs are exposed to breakage whereas the fragments of broken flocs experience re-aggregation until an equilibrium is reached, which can be observed as a constant floc size over an extended period of time [43]. When a flocculant is added to a suspension, the floc growth rate is increased causing an increase in the median chord length of flocs/particles. Irrespective to the fluctuation, the results in Fig. 2 confirms that the addition of KL-AA generated largest flocs (i.e., chord length of 85  $\mu\text{m}$ ) for the system at equilibrium

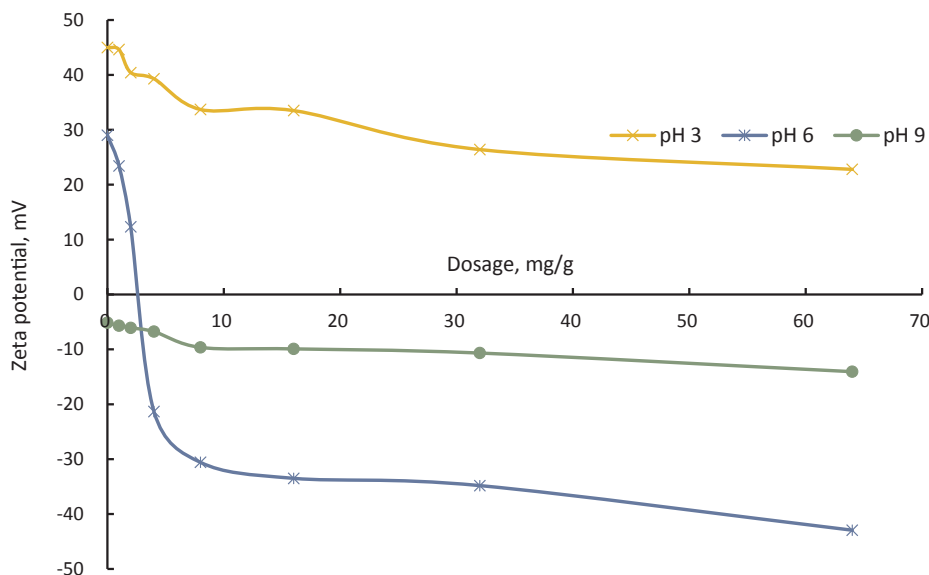


Fig. 1. Effect of KL-AA dosage on the zeta potential of aluminium oxide suspension at pH values of 3, 6 and 9.

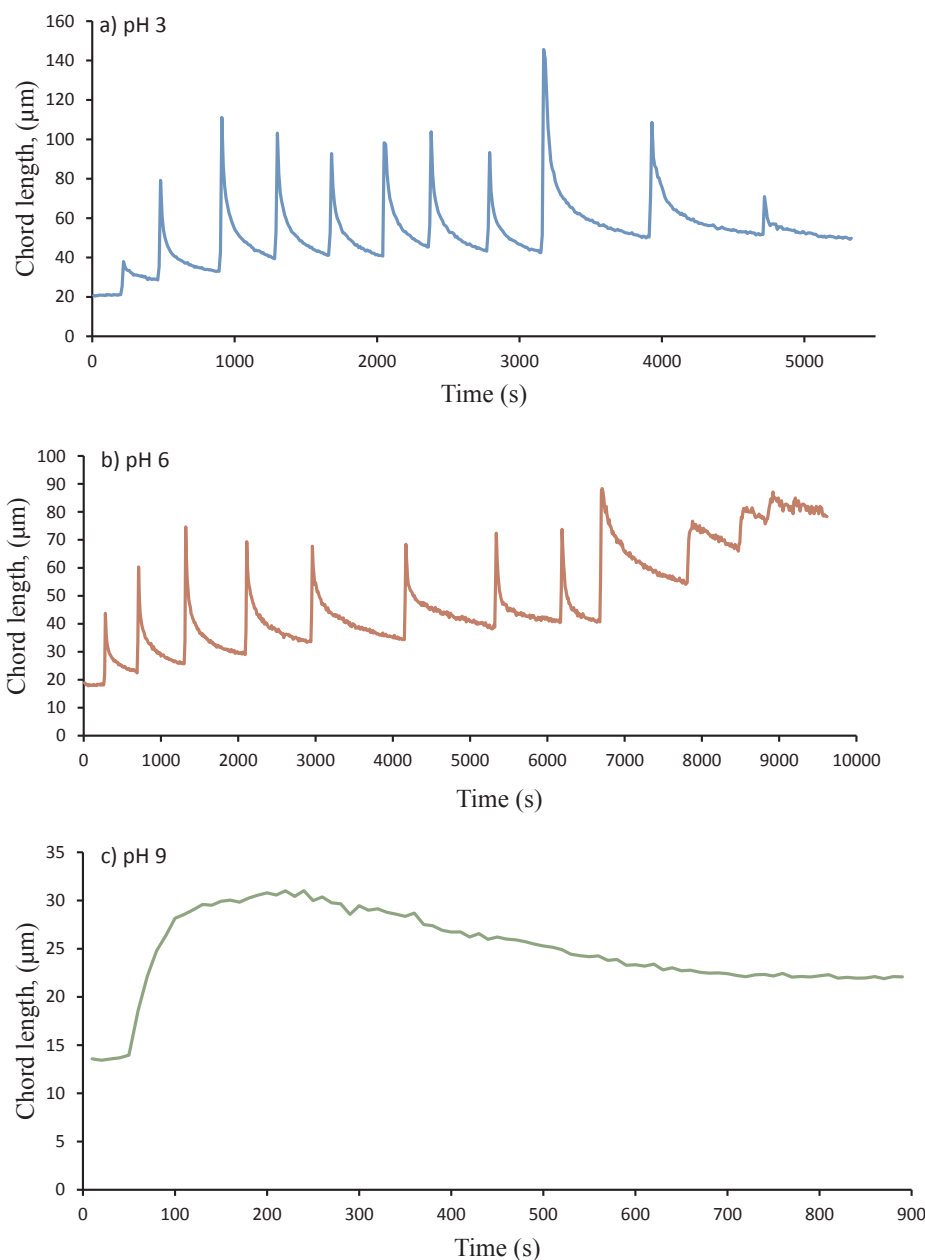


Fig. 2. Flocculation behavior of aluminium oxide suspension over time with repeated dosage of KL-AA at (a) pH 3; (b) pH 6; and (c) pH 9 in the absence of salt.

at pH 6. Blanco and coworkers studied the flocculation behavior of polyethyleneimine (PEI) in calcium carbonate suspension under shear forces and observed that the variation in the height of peaks after each polymer addition was large and the polymer induced flocs with smaller sizes that were more stable [5].

In the case of KL-AA addition at pH 3 and 6, the height of the peaks after each addition changed significantly. These results showed that the addition of KL-AA at these pH values generated large flocs, but the flocs broke after some time. As stated earlier, the large flocs are less stable and can easily breakdown under shear forces; on the contrary, the smaller particles possess more stability [5]. These results are well supported by results from zeta potential studies at pH 3 and 6, as the particles are cationically charged, but the KL-AA is anionically charged, and the polymer and particles could interact via charge interaction. At pH 9, KL-AA had a negligible effect in agglomerating particles, and it generated flocs with the smaller chord length. At pH 9, both particles and KL-AA are anionically charged (i.e., negative zeta potential in Fig. 1), and they could only interact via hydrogen bonding.

### 3.2.2. Flocculation under differing shear forces

Fig. 3(a) compares the effect of pH on the flocculation of the suspensions in the absence of salt. The results for the first 200 s corresponded to the chord length of particles in the absence of polymer. After adding KL-AA (stage 2), the polymer chains required time to disperse through the suspension, which was functions of shear forces, polymer solution viscosity and suspension concentration [52]. Then, fast flocculation occurred, which resulted in bridging particles and increasing in the chord length. However, after reaching a maximum, the median chord length decreased to an equilibrium value. As stated earlier, hydrodynamic forces originating from mixing started to break the formed flocs and the broken flocs were not able to re-agglomerate probably because of the reconfiguration of the polymers on the particle surface as well as chain scission (i.e., losing bridging efficiency) [43,52]. In stage 3 of Fig. 3, when the flocs were exposed to the high shear rates of 600 rpm, the median chord length was steeply decreased, especially for the systems with a relatively low pH. After shear rate dropped to 300 rpm (stage 4), the flocs regrew.

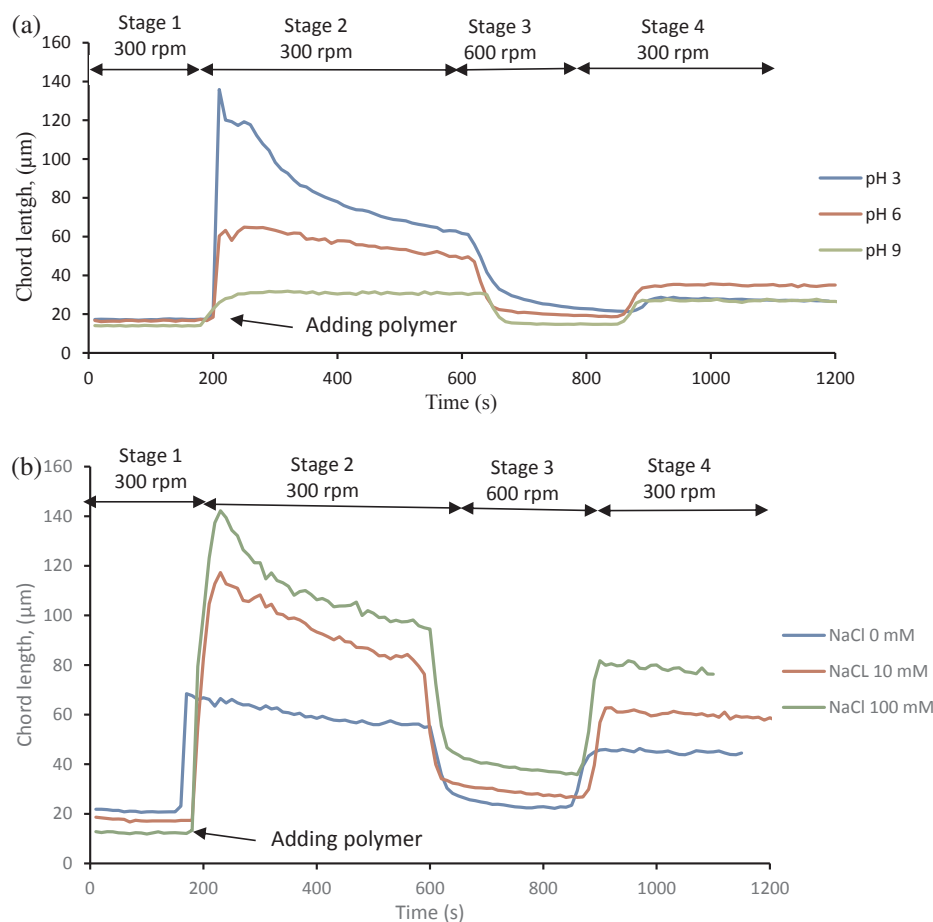


**Fig. 3.** Flocculation and de-flocculation processes for (a) KL-AA at pH 3, pH 6, and pH 9 in the absence of salt; and (b) KL-AA at pH 6 with varying salinity.

The results showed that the initial stable median chord length at pH 6 (after 600 s) is approximately 82% of the length obtained at pH 3. A further increase in alkalinity to pH 9 results in an initial stable median chord length that is merely 48% of that observed at pH 3. These results are consistent with the results in Fig. 2, as each additional point improved the chord length of flocs at pH 3 more dramatically than at pH 6. As stated earlier, the reason for this phenomenon is that at lower pH, the  $-AlOH$  groups of aluminium oxide tend to convert to positively charged  $AlOH_2^+$ , which help its fast interaction with negatively charged KL-AA. However, by increasing pH, the amount of negatively charged  $-AlO$  is significant [41]. Moreover, it is well known that the pKa of carboxylic acid is around 4.5 [16]. Therefore, increasing the pH resulted in the deprotonation of carboxylic group of AA, which increased the net negativity of the polymer. As a result, the formed aggregates repelled each other at pH 9 and flocculation efficiency reduced.

The effect of salinity was tested to determine the impact on flocculation of KL-AA. Fig. 3(b) illustrates the results obtained for the KL-AA polymer at pH 6 for three NaCl concentrations of 0, 10, and 100 mM. As the salinity of the solution increased, the stable median chord length generally increased. This behavior is explained via the principle of neutralization of particulate surface charges, which facilitates the agglomeration of particles [55]. The results illustrated in Fig. 3(b) support the hypothesis that salinity can hinder the electrostatic repulsion force created between the particles and promote the impact of KL-AA in flocculating the particles [28]. In saline systems, the charges of polyelectrolytes, including KL-AA is screened. The lack of charges on KL-AA would reduce the repulsion force generated between the segments of KL-AA already adsorbed on the surface of the particles promoting the interaction and flocculation of particles. In the same

vein, the lack of charges on aluminium oxide particle would promote the coagulation of aluminium oxide particles in the presence of salts.

### 3.2.3. De-flocculation and re-flocculation indices

In Fig. 3, as stated earlier, the stirring was intensified through an increase in impeller speed to 600 rpm (at  $t \cong 10$  min, Fig. 3); this was performed in order to induce de-flocculation. After the system achieved a stable chord length, the stirring was lessened through a decrease in impeller speed back to 300 rpm (at  $t \cong 13$ –15 min, Fig. 3). A decrease in agitation intensity was performed to induce re-flocculation in the system. Fig. 4 presents a comparison between de-flocculation and re-flocculation indices ( $DI$  and  $RI$ , respectively) for varying solution pH and salinity in the system.  $DI$  describes flocs' resistance to breakage with the onset of shear forces whilst  $RI$  describes flocs' ability to recover to the floc size with the reduction of shear forces after de-flocculation has occurred. Eqs. (1) and (2) were used to compute  $DI$  and  $RI$ , respectively, for various solution conditions, using the data of Fig. 3(a) and 3(b). Fig. 4(a) presents the  $DI$  and  $RI$  results for the systems at different pH in the absence of salt.  $DI$  are relatively similar regardless of the solution pH when the system is devoid of salt. However, there is a significant difference in the affinity of the flocs to recover their former sizes when  $RI$  is examined. The more alkaline the solution, the higher the re-flocculation index and the better the system recovers its original median chord length (Fig. 4a). At pH 3, the flocs recover to a mere 10% of their initial chord length at 300 rpm whilst at pH 9, the flocs recover to ~72% of their initial chord length. The highest recovered chord length occurred at pH 6, with a median chord length of approximately 35 μm. Although the greatest initial chord length (before inducing breakage via increasing impeller speed to 600 rpm) was observed at pH 3 (acidic conditions), the recovery for pH 3 is notably the worst and due

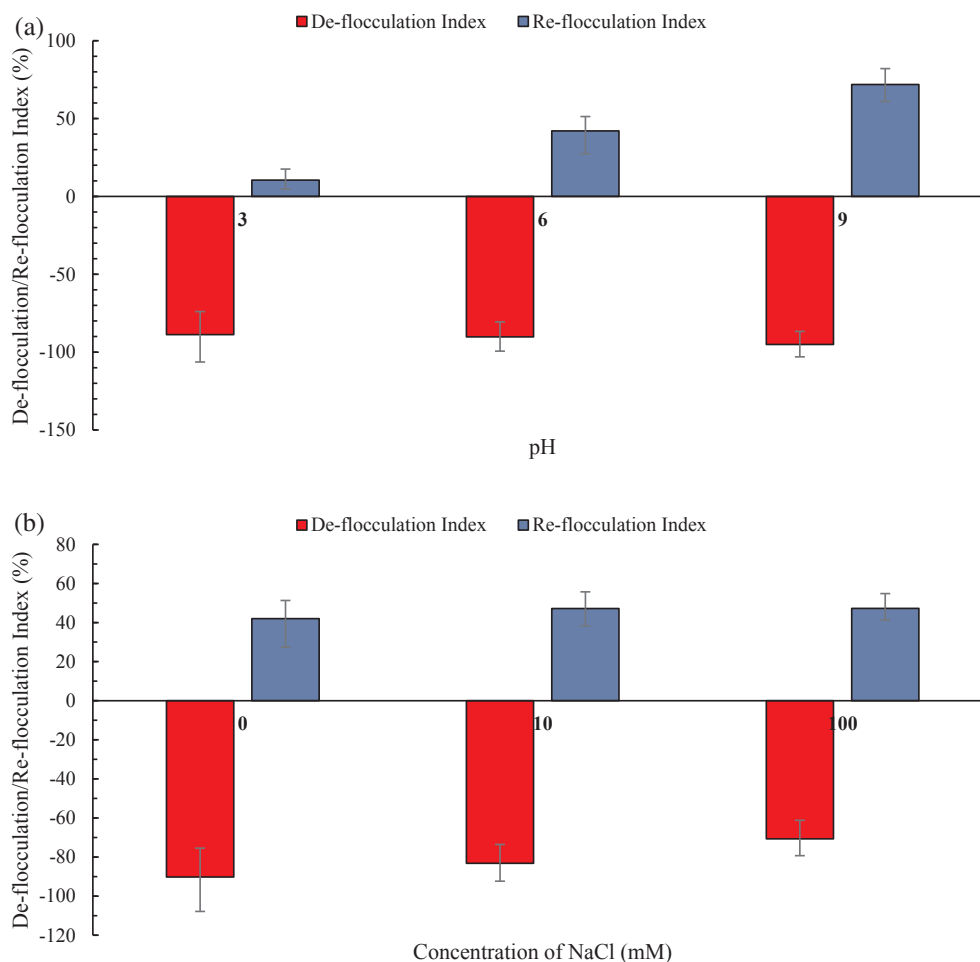


Fig. 4. De-flocculation and re-flocculation indices for aluminium oxide particles with KL-AA for (a) system at pH 3, 6, and 9 in the absence of salt; and (b) system at pH 6 in the presence of NaCl at 0, 10, and 100 mM concentrations.

to the flocs' smallest initial sizes (Fig. 3), the highest recovery occurred at pH 9.

Fig. 4(b) presents the *DI* and *RI* results for KL-AA for the system at pH 6 with varying salinity. In terms of *DI*, increased salinity appears to hinder the de-flocculation process, resulting in lesser magnitudes of *DI* with increasing NaCl concentration. The negative values for *DI* correspond to a decrease in average stable chord length from the onset of increased shear force. As concentration of NaCl increases, the flocs exhibit a greater resistance to breakage. This implies the difference in the structure of aggregates formed by the addition of various amounts of salt. It was reported that the high concentration of salt can change the configuration of polymer through reducing the thickness of the diffuse layer around the particles leading to the formation of small and compact aggregates [10]. Also, the compression of double layer resulted in the reduction of energy barrier, which enhanced attractive van der Waals forces [1]. Therefore, the compact formed flocs are more resistance to the intense shear as a result of salt addition. *RI*, however, is not significantly impacted as a result of changes in salinity, implying that the broken flocs did not have a high tendency to re-flocculate at high salinity, but the reason for this behavior is unknown to the authors (Fig. 4).

For all tests, the re-flocculation index was less than 75%, with an average recovery of ~45%. The de-flocculation index, however, was significantly high for all tests, with *DI* of up to 95% and an average *DI* of ~83%. This high breakage tendency and somewhat poor recovery are attributed to the limited bonding strength of KL-AA with particles [21]. Chaignon et al. reported that the flocs formed by bridging could not be fully recovered [12]. When flocs are broken by shear forces, changes in

the configuration of the polymer chains may occur, which hinders the re-flocculation rate [12].

### 3.3. Estimation of floc shape via probabilistic model

In addition to size, floc shape influences the collision efficiency [30] and settling velocity of the aggregated particles [22].

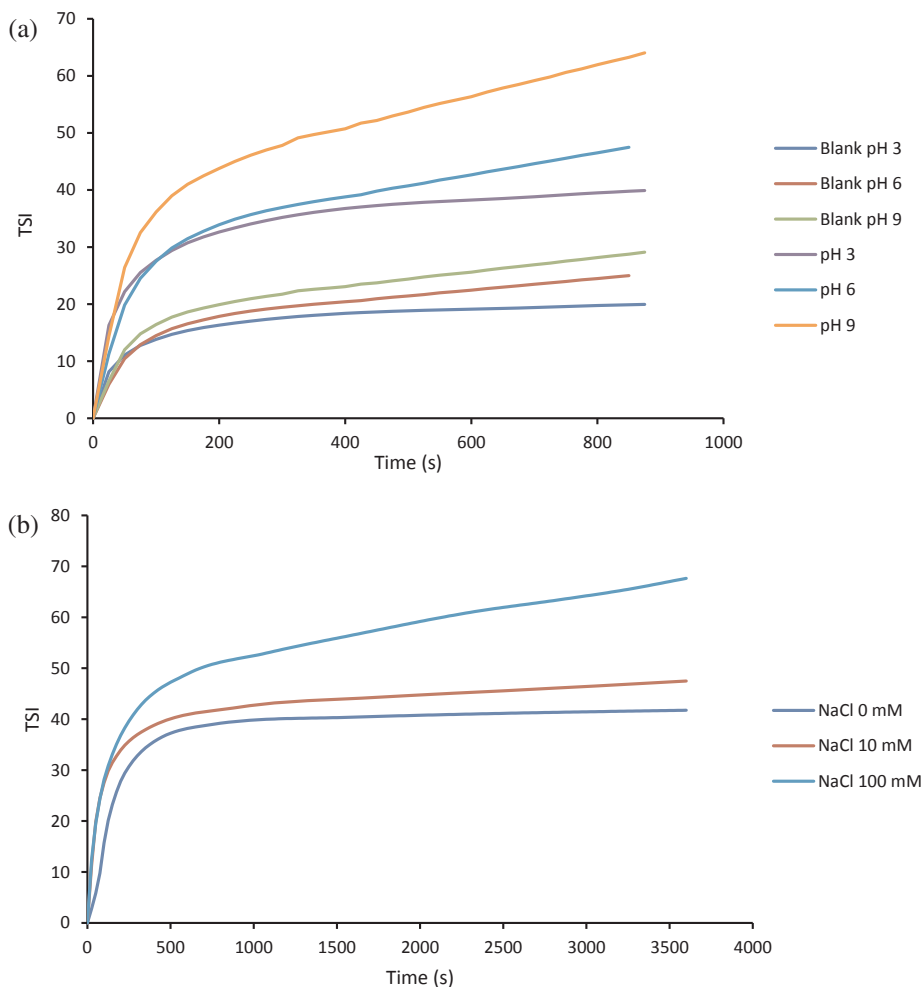
Analysis via the probabilistic model provides an inference of the heterogeneity of floc shapes for the studied systems. The shape of produced flocs influences the collision efficiency [30] and settling velocity of the aggregated particles [22]. Fig. S1 presents a sample of the results comparing the fit of the theoretical cumulative distribution curves generated at each of the three heterogeneity scenarios tested: a one-cluster regime (scenario A), a two-cluster regime (scenario B), and a three-cluster regime (scenario C). Scenario A models the mixture as being composed of one single cluster (i.e., regime), which assumes that the suspended particles are homogeneous and identical. In other words, the chord length was assumed to have only one single mode in the probability distribution function. The two-regime system modeled in scenario B assumes the suspension system contains both large-sized and small-sized particles. Scenario C demonstrates the results for a three-regime mixture model with particle sizes of three size categories. As illustrated, the three-cluster regime (scenario C) yields a better fit between the experimental results and the model (Fig. S1).

Table 1 reports the results pertaining to the solutions of shape heterogeneity analysis for flocculated aluminium oxide particles with KL-AA after initial flocculation occurs (i.e., without inducing de-flocculation or re-flocculation). In this Table,  $\delta$  is the semi-axis prolate

**Table 1**  
Heterogeneity of particle shape for KL-AA aluminium oxide suspension systems at varying pH and salinity.

Parameter	pH 3	pH 6	pH 9	NaCl 10 mM	NaCl 100 mM
<i>Scenario A: One-Cluster Regime</i>					
$\delta_1$	26.82	24.18	22.56	26.47	38.00
$\delta_1$	1.75	1.69	2.56	1.32	1.13
KL-divergence	0.02	0.03	0.01	0.04	0.005
<i>Scenario B: Two-Cluster Regime</i>					
$\pi_1$	0.49	0.72	0.42	0.51	0.32
$\pi_2$	0.51	0.28	0.58	0.49	0.70
$\delta_1$	164.19	74.62	61.27	40.16	90.12
$\delta_2$	22.54	25.94	22.06	23.92	28.91
$\epsilon_1$	2.70	1.02	1.14	1.15	1.05
$\epsilon_2$	2.82	1.44	1.147	1.53	2.43
KL-divergence	0.076	0.003	0.002	0.03	0.09
<i>Scenario C: Three-Cluster Regime</i>					
$\pi_1$	0.18	0.32	0.29	0.36	0.13
$\pi_2$	0.47	0.40	0.41	0.23	0.40
$\pi_3$	0.41	0.27	0.31	0.40	0.48
$\delta_1$	383.14	243.31	193.53	256.40	321.06
$\delta_2$	98.51	40.75	52.53	71.33	147.10
$\delta_3$	12.10	11.45	12.51	14.39	31.47
$\epsilon_1$	1.58	1.16	1.04	1.94	1.99
$\epsilon_2$	2.85	2.77	2.28	2.89	2.94
$\epsilon_3$	2.86	1.66	1.57	1.79	2.65
KL-divergence	0.0003	0.0006	0.0021	0.00067	0.0004

spheroid,  $\epsilon$  is the elongation of the spheroid, and  $\pi$  is the observed proportion of each regime. The optimal parameters ( $\delta$ ,  $\epsilon$ ,  $\pi$ ) governing each regime can be obtained by solving Eq. (4) and minimizing  $D_{KL}(p|\hat{p})$  (KL-divergence). It is evident from Table 1 that the lowest divergence occurs for regime 3; the empirical and theoretical cumulative distributions of the three-regime model has the highest goodness of fit in comparison with one and two regime models, hence it is best to assume  $\kappa = 3$  for modelling the system. The results included in Table 1 suggest that the particles had the largest size at pH 3 for all three size categories of scenario C (large, medium, small =  $\delta_1$ ,  $\delta_2$ ,  $\delta_3$ ). In addition to the diameter of the three size categories for scenario C, the shapes of the flocs must deviated from spheres for the probabilistic model to agree with the experimental results (i.e.,  $\epsilon_1$ ,  $\epsilon_2$ ,  $\epsilon_3 > 1$ ). In Table 1, as pH increases, the deviations from  $\epsilon = 1$  is lessened. It is worth mentioning that spherical particles are obtained when the elongation  $\epsilon$  approaches to one (for any prolate spheroid,  $\epsilon > 1$ ). For pH 3, the results suggest that the shape of large-sized particles minimally deviate from spheres as the maximum likelihood estimator for their elongation is obtained to be 1.58. Also, the shapes of the small-sized and medium-sized particles ( $\delta = 12.10 \mu\text{m}$  and  $98.51 \mu\text{m}$ , respectively) deviate significantly from spheres since  $\epsilon = 2.86$  and  $2.85$  are substantially greater than  $\epsilon = 1$ . By increasing the pH from 3 to 9, the particles are more likely to possess more spherical shapes since their corresponding elongations decrease as indicated by the model. In fact, the system shows a tendency to become more stable via particle coarsening and spheroidization. It is also worth mentioning that larger and spherical particles have the least surface energy and hence the lower total free



**Fig. 5.** TSI of aluminium oxide/KL-AA suspension for (a) pH of 3, 6, and 9 (no salinity) including control samples (i.e., no KL-AA); and (b) solution NaCl concentrations of 0, 10, and 100 mM at pH 6.

**Table 2**  
Settling velocity and sedimentation of the formed flocs at various pH and salinity after 1 h of measurement.

Label	Sediment concentration (g/L)	Settling velocity (mm/h)
Blank-pH 3	92.24	155.31
Blank-pH 6	95.76	178.01
Blank-pH 9	145.18	196.6
Sample-pH 3	45.72	232.9
Sample-pH 6	50.12	253.8
Sample-pH 9	108.48	281.3
Sample-NaCl 10 mM	52.97	301.52
Sample-NaCl 100 mM	60.12	370.84

energy [47].

Table 1 also discloses the parameters for each scenario for the saline systems. An increase in the concentration of salt necessitates an increase in the size of all three bins for scenario C modelling ( $\delta_1$ ,  $\delta_2$ ,  $\delta_3$ ; Table 1). High salinity may neutralize the surface charges of particles and therefore increase the agglomeration of particles [55], resulting in a cumulative size distribution that encompasses relatively larger sized particles. For the sample with no salt (0 mM NaCl, Table 1), the numerical results suggest that the large-sized particles would have shapes relatively closer to spheres since the maximum likelihood estimator for their elongation is 1.16 (i.e., close to 1). Moreover, by increasing the concentration of NaCl, the particles are predicted to possess less spherical shapes since their corresponding elongations increased.

### 3.4. Flocculation under non-stirring conditions

Fig. 5(a) shows the Turbiscan Stability Index (TSI) value of the aluminium oxide suspension as a function of time under non-stirring condition. The greater the value of TSI at a given time, the poorer the stability of the system would be. In terms of blank samples, the results depicted that aluminium oxide suspension was more unstable at pH 9, this pH being close to the solution's isoelectric point (zeta potential of  $-5$  mV, Fig. 1). As shown in Fig. 5(a), adding KL-AA to the system destabilized the system in general, facilitating settling of particles. The addition of KL-AA to the system at pH 3 resulted in the least instability for the aluminium oxide suspension system, whilst the greatest instability occurs at pH 9. Fig. 5(b) shows the TSI value of the aluminium oxide suspension as a function of time under the non-stirring condition for samples at different salt concentrations. It is evident that an increase in the salinity for the system results in increasing instability for the system. These results are consistent with literature reports [29] supporting the concept that increasing the salt concentration improves the settling of particles.

The settling velocity and the compactness of sediments after 60 min of settling are compared in Table 2. The settling velocity is described as the growth rate of sediment thickness [26,51]. Blank aluminium oxide suspensions experienced slower settling velocities than did the KL-AA containing systems at pH 3 (Table 2) due to their high zeta potential (Fig. 1). Also, the alkaline condition (pH 9) resulted in the highest settling velocity ( $\sim 281$  mm/h), which may be related to their shape (Table 1). Flocs with more spherical shapes settle faster in general [26]. In terms of sediment concentration, the blank systems exhibited the highest sediment concentrations; and the addition of KL-AA decreased the sediment concentration at all pH (Table 2). These results also confirm that the weak flocs at pH 3 generated sediment with lowest concentration and higher porosity. These results may suggest that these large flocs risk entraining water. Vajihinejad and Soares [52] claimed that polyacrylamide (PAM) based flocculants could generate a loose precipitate and gel-like structure that capture water [52].

Table 2 also presents the settling velocities and sediment concentrations for the KL-AA aluminium oxide solution as a function of

salinity. In terms of settling velocity, the addition of salt to the KL-AA aluminium oxide solution increased settling velocities (Table 2), which is in good agreement with the results reported by Ji et al. [29]. The addition of salt serves to decrease the intramolecular electrostatic repulsion force between negatively charged particles, which allows for larger flocculated particles with a higher settling velocity [46]. Also, the suspension without salt (0 mM NaCl) had the lowest sediment concentration ( $\sim 50$  g/L), with the addition of salt increasing the concentration of the sediment.

## 4. Conclusions

The results showed that the decrease in zeta potential was most pronounced at pH 6. The interaction of KL-AA with particles generated the largest flocs at pH 3. However, the flocs could not be recovered after de-flocculation/re-flocculation, as the interaction of KL-AA and the particles were weak at this pH. These flocs generated sediment with lowest concentration. At pH 6, the charge interaction and bridging generated the largest flocs. These flocs had stronger tendency to recover their sizes after re-flocculation. At pH 9, due to limited interaction (primarily due to hydrogen bonding), small but recoverable flocs were mainly generated, which led to sediment with the highest concentration. A numerical heterogeneity study concerning particle size and shapes reveals that a three-cluster particle regime best reproduced the experimental chord length distributions for all experiments. Increasing pH reduced the particle diameter and elongation providing evidence for the generation of more compact and spherical shape particles.

Also, the median chord length increased as a result of increasing salinity. Concentrating salinity resulted in an increase in particle diameter and elongation (or deviation from spherical clusters). The flocs seem to be slightly stronger at higher salinity. The salt seems to increase the concentration of sediment, even though the sediments had generally very low concentrations. TSI results also confirmed increased instability and higher settling rate at higher pH and salinity. Overall, this work showed mathematically and experimentally how a novel biobased flocculant, KL-AA, could function in altered environments (i.e., pH and salt concentration). As pH and salt are two important parameters of industrial effluents, this work would depict the potential performance of KL-AA in industrial effluents.

### CRedit authorship contribution statement

**Minoo Ataie:** Formal analysis, Methodology, Validation, Software, Investigation, Writing - original draft. **Kayte Sutherland:** Validation, Methodology, Software, Investigation, Writing - review & editing. **Leila Pakzad:** Validation, Supervision. **Pedram Fatehi:** Conceptualization, Supervision.

### Acknowledgements

The authors would like to acknowledge NSERC, Canada Foundation for Innovation, Canada Research Chairs and Northern Ontario Heritage Fund Corporation programs for their valuable financial support. Also, assistance from Sanaz Sabaghi is acknowledged.

### Appendix A. Supplementary material

Supplementary data to this article can be found online at <https://doi.org/10.1016/j.seppur.2020.116944>.

### References

- [1] B. Alinec, T.G.M. Van de Ven, Stability of clay suspensions—effect of pH and polyethylenimine, *J. Colloid Interface Sci.* 155 (2) (1993) 465–470.
- [3] E. Arinaitwe, M. Pawlik, A role of flocculant chain flexibility in flocculation of fine quartz. Part I. A role of flocculant chain flexibility in flocculation of fine quartz. Part

- I. Intrinsic viscosities of polyacrylamide-based flocculants, *Int. J. Miner. Process.* 124 (2013) 50–57.
- [4] L. Besra, D. Sengupta, S. Roy, P. Ay, Influence of surfactants on flocculation de-watering of kaolin suspensions by cationic polyacrylamide (PAM-C) flocculant, *Sep. Purif. Technol.* 30 (2003) 251–264.
- [5] A. Blanco, E. Fuente, C. Nergo, J. Tijero, Flocculation monitoring: focused beam reflectance measurement as a measurement tool, *Can. J. Chem. Eng.* 80 (2002) 1–7.
- [6] J.A. Boxall, C.A. Koh, E.D. Sloan, A.K. Sum, D.T. Wu, Droplet size scaling of water-in-oil emulsions under turbulent flow, *Langmuir* 28 (2011) 104–110.
- [7] G. Bronow, Method to reveal the structure of lignin, biopolymer: lignin, humic substances and coal. Edited by M Horfricher and A Steinbuechel. Wiley-VCH. Weinheim, 2001, pp. 93–112.
- [8] B.C. Cao, B.Y. Gao, X. Liu, M.M. Wang, Z.L. Yang, Q.Y. Yue, The impact of pH on floc structure characteristic of polyferric chloride in low DOC and high alkalinity surface water treatment, *Water Res.* 45 (18) (2011) 6181–6188.
- [9] M. Castelnuovo, J.F. Joanny, Formation of polyelectrolyte multilayers, *Langmuir* 16 (2000) 7524–7532.
- [10] M. Cadotte, M.E. Tellier, A. Blanco, E. Fuente, T.G. Van De Ven, J. Paris, Flocculation, retention and drainage in papermaking: a comparative study of polymeric additives, *Can. J. Chem. Eng.* 85 (2) (2007) 240–248.
- [11] R.K. Chakraborti, J.F. Atkinson, J.E. Van Benschoten, Characterization of alum floc by image analysis, *Environ. Sci. Technol.* 34 (18) (2000) 3969–3976.
- [12] V. Chaignon, B.S. Lartiges, A. El Samrani, C. Mustin, Evolution of size distribution and transfer of mineral particles between flocs in activated sludges: an insight into flocs exchange dynamics, *Water Res.* 36 (3) (2002) 476–484.
- [14] R.L. Chen, B.V. Kakta, C. Daneault, J.L. Valade, Some water-soluble copolymers from lignin, *Appl. Polym. Sci.* 18 (1986) 1559–1564.
- [15] S. Chibowski, M. Wiśniewska, T. Urban, Influence of solution pH on stability of aluminium oxide suspension in presence of polyacrylic acid, *Adsorption* 16 (2010) 321–332.
- [16] K.K. Das, P. Somasundaran, Flocculation-dispersion characteristics of alumina using wide molecular weight range of polyacrylic acids, *Colloid Surf. A* 223 (2003) 17–25.
- [17] E.A. El-Katany, S.A. Halawy, M.A. Mohamed, M.I. Zaki, Recovery of high surface area alumina from aluminium dross tailings, *J. Chem. Technol. Biotechnol.: Int. Res. Process. Environ. Clean Technol.* 75 (5) (2000) 394–402.
- [18] P. Fatehi, W. Gao, Y. Sun, M. Dashban, Acidification of prehydrolysis liquor and spent liquor of neutral sulfite semichemical pulping process, *Bioresour. Technol.* 218 (2016) 518–525.
- [19] S.B. Francois, Strength of aluminium hydroxide flocs, *Water Res.* 21 (1987) 1023–1030.
- [20] G. Franks, Stimulant sensitive flocculation and consolidation for improved solid/liquid separation, *J. Colloid Interface Sci.* 292 (2005) 598–603.
- [21] J.E. Gebhardt, D.W. Fuerstenau, Flotation behavior of hematite fines flocculated with polyacrylic acid, *Miner. Metall. Process.* 3 (1986) 164–170.
- [22] B. Gorczyca, J. Ganczarzyk, *Environ. Technol.* 17 (1996) 1361–1369.
- [23] X. Guo, D. Xiang, G. Duan, P. Mou, A review of mechanochemistry applications in waste management, *Waste Manage.* 30 (1) (2010) 4–10.
- [24] A. Hasan, P. Fatehi, Stability of kaolin dispersion in the presence of lignin-acrylamide polymer, *Appl. Clay Sci.* 158 (2018) 72–82.
- [25] W. He, Y. Zhang, P. Fatehi, Sulfomethylated kraft lignin as a flocculant for cationic dye, *Colloid Surf. A* 503 (2016) 19–27.
- [26] A.R. Heath, P.A. Bahri, P.D. Fawell, J.B. Farrow, Polymer flocculation of calcite: relating the aggregate size to the settling rate, *Am. Inst. Chem. Eng. J.* 52 (2006) 1987–1994.
- [27] P. Jarvis, B. Jefferson, J. Gregory, S.A. Parsons, A review of floc strength and breakage, *Water Res.* 39 (14) (2005) 3121–3137.
- [28] R.I. Jeldres, E.C. Picerros, W.H. Leiva, P.G. Toled, N. Herrera, Viscoelasticity and yielding properties of flocculated kaolinite sediments in saline water, *Colloid Surf. A* 529 (2017) 1009–1015.
- [29] Y. Ji, Q. Lu, Q. Liu, H. Zeng, Effect of solution salinity on settling of mineral tailings by polymer flocculants, *Colloid Surf. A* 24 (2013) 29–38.
- [30] Q. Jiang, B. Logan, Fractal dimensions of aggregates determined from steady-state size distributions, *Environ. Sci. Technol.* 25 (12) (1991) 2031–2038.
- [31] M.K. Konduri, P. Fatehi, Dispersion of kaolin particles with carboxymethylated xylan, *Appl. Clay Sci.* 137 (2017) 183–191.
- [32] F. Kong, S. Wang, J.T. Price, M.K. Konduri, P. Fatehi, Water soluble kraft lignin-acrylic acid copolymer: synthesis and characterization, *Green Chemistry* 17 (2015) 4355–4366.
- [33] F. Kong, S. Wang, W. Gao, P. Fatehi, Novel pathway to produce high molecular weight kraft lignin-acrylic acid polymers in acidic suspension systems, *The Royal Soc. Chem.* 8 (2018) 12322–12336.
- [34] S. Kullback, R.A. Leibler, On information and sufficiency, *Ann. Math. Statistics* 22 (1951) 79–86, <https://doi.org/10.1214/aoms/1177729694>.
- [35] C.S. Lee, J. Robinson, M.F. Chong, A review on application of flocculants in wastewater treatment, *Process Saf. Environ. Prot.* 92 (6) (2014) 489–508.
- [36] S. Li, L. Gao, Y. Cao, X. Gui, Z. Li, Effect of pH on the flocculation behaviors of kaolin using a pH-sensitive copolymer, *Water Sci. Technol.* 74.3 (2016) 729–737.
- [37] C. Mai, O. Milstein, A. Huttermann, Chemoenzymatical grafting of acrylamide onto lignin, *J. Biotechnol.* 79 (2000) 173–183.
- [38] J.J. Meister, A. Lathia, F.F. Chang, Solvent effects, species and extraction method effects, and coinitiator effect in the grafting of lignin, *Macromolecules* 18 (1985) 1559–1564.
- [39] O. Mengual, G. Meunier, I. Cayré, K. Puech, P. Snabre, Turbiscan ma 2000: multiple light scattering measurement for concentrated emulsion and suspension instability analysis, *Talanta* 50 (1999) 445–456.
- [40] P. Mporfu, J. Addai-Mensah, J. Ralston, Investigation of the effect of polymer structure type on flocculation, rheology and dewatering behavior of kaolinite dispersions, *Int. J. Miner. Process.* 71 (2003) 247–268.
- [41] M.S. Nasser, A.E. James, The effect of polyacrylamide charge density and molecular weight on the flocculation and sedimentation behaviour of kaolinite suspensions, *Sep. Purif. Technol.* 52 (2006) 241–252.
- [42] R. Nicu, E. Bobu, R. Miranda, A. Blanco, Flocculation efficiency of chitosan for papermaking applications, *BioResources* 8 (1) (2013) 768–784.
- [43] B. Oyegebile, P. Ay, S. Narra, Flocculation kinetics and hydrodynamic interactions in natural and engineered flow systems: A review, *Environ. Eng. Res.* 21 (1) (2016) 1–14.
- [44] S. Pal, G. Sen, N.C. Karmakar, D. Mal, R.P. Singh, High performance flocculating agents based on cationic polysaccharides in relation to coal fine suspension, *Carbohydrate Polym.* 74 (2008) 590–596.
- [45] M. Pearse, An overview of the use of chemical reagents in mineral processing, *Miner. Eng.* 18 (2005) 139–149.
- [46] L.I. Portela, S. Ramos, A.T. Teixeira, Effect of salinity on the settling velocity of fine sediments of a harbour basin, *J. Coastal Res.* 65 (sp2) (2013) 1188–1194.
- [47] D.A. Porter, K.E. Easterling, M. Sherif, Phase Transformations in Metals and Alloys, (Revised Reprint). CRC Press, 2009.
- [48] C. Rattanakawin, R. Hogg, Aggregate size distribution in flocculation, *Colloids Surf. A: Physicochem. Eng.* 177 (2001) 87–98.
- [49] H. Rong, B. Gao, Y. Zhao, S. Sun, Z. Yang, Y. Wang, Q. Yue, Q. Li, Advanced lignin-acrylamide water treatment agent by pulp and paper industrial sludge: Synthesis, properties and application, *J. Environ. Sci.* 25 (12) (2013) 2367–2377.
- [50] N. Tambo, H. Hozumi, Physical characteristics of flocs II: Strength of floc, *Water Res.* 13 (1979) 421–428.
- [51] P. Tong, B.J. Ackerson, Analogies between colloidal sedimentation and turbulent convection at high prandtl numbers, *Phys. Rev. E* 58 (1998) R6931.
- [52] V. Vajihinejad, J.B.P. Soares, Monitoring polymer flocculation in oil sands tailings: A population balance model approach, *Chem. Eng. J.* 346 (2018) 447–457.
- [53] S. Wang, Y. Sun, F. Kong, G. Yang, P. Fatehi, Preparation and characterization of lignin-acrylamide copolymer as a paper strength additive, *Bioresources* 11 (1) (2016) 1765–1783.
- [54] M. Wiśniewska, S. Chibowski, T. Urban, Adsorption and thermodynamic properties of the alumina-polyacrylic acid solution system, *J. Colloid Interface Sci.* 334 (2) (2009) 146–152.
- [55] Wu, M.R., Van de ven, T.G.M. 2009. Flocculation and reflocculation: Interplay between the adsorption behavior of the components of a dual flocculant. *Physicochem. Eng. Aspects* 341, 40–45.
- [57] A.K. Yeung, R. Pelton, Micromechanics: a new approach to studying the strength and break up of flocs, *Colloid Interface Sci.* 184 (2) (1996) 579–585.
- [58] X. Yu, P. Somasundaran, Enhanced flocculation with double flocculants, *Colloids Surf., A* 81 (1993) 17–23.
- [59] W.Z. Yu, G.B. Li, Y.P. Xu, X. Yang, Breakage and re-growth of flocs formed by alum and PACL, *Powder Technol.* 189 (2009) 439–443.
- [60] X. Yu, P. Somasundaran, Role of polymer conformation in interparticle-bridging dominated flocculation, *J. Colloid Interface Sci.* 177 (2) (1996) 283–287.
- [61] Y. Zhang, W. Gao, P. Fatehi, Structure and settling performance of aluminium oxide and poly acrylic acid flocs in suspension systems, *Sep. Purif. Technol.* 215 (2019) 115–124.